PCCP

PAPER

View Article Online
View Journal | View Issue

Cite this: *Phys. Chem. Chem. Phys.*, 2014, **16**, 18781

High-field liquid state NMR hyperpolarization: a combined DNP/NMRD approach†

Petr Neugebauer,[a] Jan G. Krummenacker,[a] Vasyl P. Denysenkov,[a] Christina Helmling,[a] Claudio Luchinat,[b] Giacomo Parigi*[b] and Thomas F. Prisner*[a]

Received 4th June 2014,
Accepted 15th July 2014

DOI: 10.1039/c4cp02451f

www.rsc.org/pccp

Here we show how fast dynamics between radicals and solvent molecules in liquid solutions can be detected by comparison of coupling factors determined by nuclear magnetic relaxation dispersion (NMRD) measurements and dynamic nuclear polarization (DNP) enhancement measurements at high magnetic field (9.2 T). This is important for a theoretical understanding of the Overhauser DNP mechanism at high magnetic fields and thus for optimization of the DNP agent/target system for high resolution liquid state NMR applications. Mixtures of the solution of TEMPOL radicals in water, toluene, acetone and DMSO have been investigated. The results are compared to the classical hard-sphere model and molecular dynamic simulations. Our results clearly indicate that fast sub-ps dynamics, which are not related to classical rotational or translational motion of the molecules, significantly contribute to the Overhauser DNP mechanism at high magnetic fields.

Introduction

It has been shown that dynamic nuclear polarization (DNP) can significantly enhance NMR signals in solids even at high magnetic fields.[1] The mechanisms responsible for this polarization transfer in solids are the solid effect in the case of a spin $S = 1/2$, $I = 1/2$ system and the cross effect if two radicals couple simultaneously to the nuclear spin. Fast dissolution of the solid after DNP polarization transfer allows one to use this hyperpolarization for ^{13}C MRI and MRS applications in liquids.[2] Subsequently also surprisingly large DNP enhancements have been observed in liquids at magnetic fields of 9.2 T (corresponding to 400 MHz proton NMR frequency).[3,4] In this case the DNP enhancement is based on the unbalance of the cross-relaxation rates (zero-quantum and double quantum) between nuclear and electron spin and the mechanism is called Overhauser effect.[5] The Overhauser enhancement can be written as

$$\varepsilon_{OE} = \frac{\langle I_z \rangle - I_0}{I_0} = \frac{\gamma_e}{\gamma_n} \cdot f \cdot s \cdot \xi \qquad (1)$$

where γ_e and γ_n are the gyromagnetic ratios of the electron and the nucleus, respectively, *i.e.* $\gamma_e/\gamma_n \approx -660$ for a proton spin, and $f = 1 - T_{1IS}/T_{1I}$ is the leakage factor, which can be determined from the nuclear T_1 relaxation time in the presence (T_{1IS}) or absence (T_{1I}) of radicals in the solution. It denotes how much of the relaxation of the nuclear spin is caused by the radicals ($f = 1$ for 100%, $f = 0$ for 0%). The saturation factor s describes how well the electron spin system is saturated by the resonant microwave (MW) irradiation, ranging again from 0 (no saturation) to 1 (full saturation). The last parameter ξ is called the coupling factor. While f can be optimized by varying the concentration of the radical and s by applying enough microwave power, the coupling factor ξ depends on the strength and dynamics of the coupling between electron and nuclear spin and cannot be easily controlled. For magnetic dipole–dipole coupling, which is usually the dominant coupling for radicals and proton nuclear spins of solvent molecules, the maximum coupling factor is $\xi = 0.5$. This yields a maximal theoretical enhancement of -330 for proton nuclear spins. Whereas the leakage factor f can be easily determined by NMR experiments, the saturation factor s is more difficult to access at high magnetic fields in solutions. We found recently that for high radical concentrations the quenching of the paramagnetic shift can be used to determine this value.[6] The coupling factor ξ can be calculated from the spectral density function $J(\omega)$ of the dipolar interaction by

$$\xi = \frac{5J(\omega_s)}{3J(\omega_I) + 7J(\omega_s)} \qquad (2)$$

where ω_s and ω_I are the electron and nuclear spin Larmor frequencies, respectively. Within the force-free hard sphere

[a] *Institute of Physical and Theoretical Chemistry and Center for Biomolecular Magnetic Resonance (BMRZ), Goethe-University, Max-von-Laue-Str. 7, 60438, Frankfurt am Main, Germany. E-mail: prisner@chemie.uni-frankfurt.de*
[b] *Magnetic Resonance Center (CERM) and Department of Chemistry, University of Florence, Via L. Sacconi 6, Florence, Italy. E-mail: parigi@cerm.unifi.it*

† Electronic supplementary information (ESI) available. See DOI: 10.1039/c4cp02451f

model[7] the spectral density function for translational diffusion can be expressed by

$$\tilde{J}(\omega,\tau) = \frac{1 + 5z/8 + z^2/8}{1 + z + z^2/2 + z^3/6 + 4z^4/81 + z^5/81 + z^6/648} \quad (3)$$

with $z = (2\omega\ \tau_D)^{1/2}$ and the diffusion correlation time τ_D given by

$$\tau_D = \frac{d^2}{D} \quad (4)$$

with D being the sum of the diffusion coefficients of the radical and the solvent molecule and d the distance of closest approach between electron and nuclear spin. More sophisticated models also include an inner-sphere contribution from the rotation of the transient radical–solvent complex with a rotational correlation time τ_R.[8] The respective correlation times can be determined from the field dependence of the solvent proton relaxation dispersion (NMRD) profiles.[8,9]

Recently we could show that the DNP enhancement at a magnetic field of 9.2 T of a solution of TEMPOL in water could be quantitatively modelled by the translational motion of nitroxide and water molecules and an additional contribution arising from a fast motion, which could be modelled within the classical force-free hard-sphere model by a fast inner-sphere rotation of the complex.[6] Molecular dynamic simulations of TEMPOL in water also suggested contributions from fast local dynamics of the TEMPOL–water complex.[10] Here we extended this study to the solvents acetone, toluene and DMSO. Despite the fact that these solvents have rather different viscosities and diffusion rates, substantial DNP enhancements have been observed for all solvents. Comparison of the high field DNP enhancements with the NMRD measurements allows us to conclude that additional fast dynamics of the radical–solvent complex contribute substantially to the coupling factor at high magnetic fields.

Results and discussion

Solutions of TEMPOL (4-hydroxy-2,2,6,6-tetramethylpiperidin-1-oxyl) radicals with the solvents shown in Scheme 1 were prepared with different radical concentrations (5 mM–1 M). Samples were filled in the respective capillaries for NMR, EPR or DNP experiments without degassing.

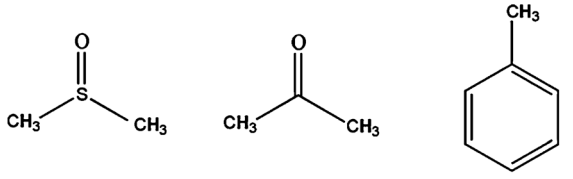

DMSO	Acetone	Toluene
$0.73 \cdot 10^{-9}$ m^{2}s^{-1}	$4.57 \cdot 10^{-9}$ m^{2}s^{-1}	$2.27 \cdot 10^{-9}$ m^{2}s^{-1}
189 °C	57 °C	111 °C

Scheme 1 Solvent molecules used in this study together with their diffusion coefficients at 25 °C and their boiling points in °C.

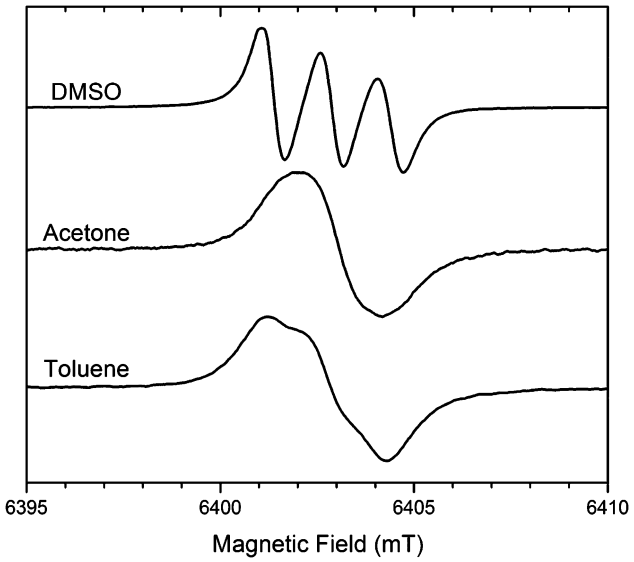

Fig. 1 180 GHz CW-EPR spectra of 40 mM ^{14}N-TEMPOL in DMSO, acetone and toluene samples (not degassed) recorded at room temperature. The picture shows the varied line shape broadening for all three solvents, due to the different Heisenberg exchange rates.

Because of the rather different diffusion coefficients of the solvents, different EPR spectra and DNP enhancements are expected at high magnetic fields. Fig. 1 shows CW-EPR spectra taken at 180 GHz (G-band) for 40 mM ^{14}N-TEMPOL concentrations recorded at a temperature of 25 °C.

The linewidth is affected by the presence of paramagnetic oxygen in the sample. Whereas in the case of DMSO the amount of dissolved oxygen is negligible (0.034 ml O_2 ml^{-1} solvent)[11] this is not the case for acetone (0.207 ml O_2 ml^{-1} solvent)[12] and toluene (0.186 ml O_2 ml^{-1} solvent).[13] However at high fields the contribution of oxygen to the linewidth is less pronounced than at 9 GHz (X-band) frequencies where even a small amount of paramagnetic oxygen affects the linewidth strongly. The main difference of the line shape for the different solvents thus comes from Heisenberg spin exchange, demonstrating the rather different translational dynamics of the different solutions. We extracted spin exchange rates from linewidth broadening as a function of radical concentration at X- and G-band frequencies. Values for the exchange rate of $k_H = (2.7 \pm 0.1) \times 10^{-9}$ M^{-1} s^{-1}, $(11.2 \pm 0.2) \times 10^{-9}$ M^{-1} s^{-1} and $(8.8 \pm 0.3) \times 10^{-9}$ M^{-1} s^{-1} for DMSO, acetone and toluene, respectively, were determined at 25 °C. At higher temperature and concentration the three lines collapse into a single line which narrows further before finally dipolar line broadening occurs at very high concentrations (see ESI†).

The DNP experiments were performed over a broad range of ^{14}N-TEMPOL radical concentrations: from 5 mM up to 1 M in the case of DMSO and acetone or up to 200 mM in the case of toluene. Fig. 2 shows DNP experiments performed on a sample doped with 1 M ^{14}N-TEMPOL in DMSO (Fig. 2A, 30 μm ID capillary size), in acetone (Fig. 2B, 20 μm ID capillary size) and in toluene (Fig. 2C, 50 μm ID capillary size). The irradiation MW power was approximately 450 mW in all experiments,

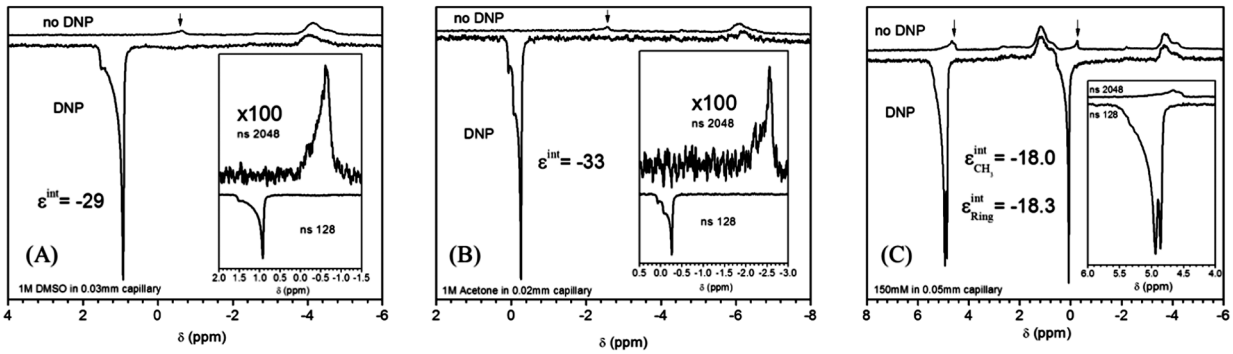

Fig. 2 Normalized ^{1}H-NMR spectra to single scan of 1 M ^{14}N-TEMPOL in DMSO (A), acetone (B) and toluene (C) with (lower spectrum −128 scans) and without (upper spectrum −2048 scans) MW irradiation of the sample. Spectral intensities are normalized to number of scans. An integrated enhancement of −29, −33 and −18.3 can be observed on the corresponding proton signals. The inset shows the reference spectrum without irradiation enlarged by a factor of 100 for comparison, except toluene (C) where the detail of the enhanced aromatic ring is shown. The peak at −4 ppm arises from solvent outside of the MW-resonator and is therefore not enhanced.

corresponding to a B_1 field of 3 G. All microwave pumped signals show a strong negative enhancement, as expected for dipolar coupling. Enhancement factors ε are −29, −33 and −18 for DMSO, acetone and toluene, respectively.

Notably, while the signal from outside of the MW cavity remains unchanged at the same position, the DNP enhanced signal significantly changes its position with respect to the reference signal as indicated by the arrows in the figure. This shift, as already explained in our previous work on water,[6] is caused by a combination of MW heating and strong paramagnetic shift[14] induced by the high radical concentration. Therefore it is important to know temperature as well as the saturation factor for a quantitative evaluation of the DNP results. Whereas in DMSO and acetone we resolved only the signal from the methyl groups, in the case of the toluene sample (Fig. 2C) we were able to resolve all three signals, even if the resolution of the DNP probe is not optimal yet. We observed two signals from hydrogens bound to the aromatic ring and one signal from the methyl group (aliphatic hydrogens). The overall integrated enhancement of the ring protons is slightly larger compared to that of the methyl groups (Fig. 2C). In Fig. 3, the measured NMR signal enhancements for all three samples are shown as a function of applied microwave power.

In all cases the enhancement rises monotonically with increasing microwave power, due to the increased temperature of the sample. Saturation of the EPR transition is achieved for these concentrations of radicals already much earlier, as reflected by the suppression of the paramagnetic shift as a function of microwave power (see ESI†). Therefore the saturation factor is $s \approx 1$.

The leakage factor was measured for all solvents and concentrations in the temperature range where DNP experiments were performed. Table 1 shows leakage factors at room temperature (25 °C). Despite the fact that again all solvents exhibit different concentration dependence of the leakage factor, for concentrations above 100 mM the leakage factor under DNP conditions is $f \approx 1$ for all solvents and experimental temperatures (more information in ESI†). The estimation of the saturation factor and the leakage factor is important (see eqn (1)) for determining the coupling factors related to the measured DNP enhancements ε. In this way, the coupling factors obtained from DNP and NMRD measurements can be quantitatively compared.

Table 1 Measured leakage factor f as a function of ^{14}N-TEMPOL concentration at 25 °C for organic solvents used as well as for water

	200 mM	100 mM	40 mM	20 mM	5 mM
DMSO	0.99	0.98	0.95	0.89	0.69
Acetone	0.98	0.93	0.85	0.62	0.26
Toluene CH_3/ring	0.98/0.99	0.96/0.98	0.91/0.94	0.85/0.89	0.58/0.67
Water	0.99	0.98	0.95	0.90	0.66

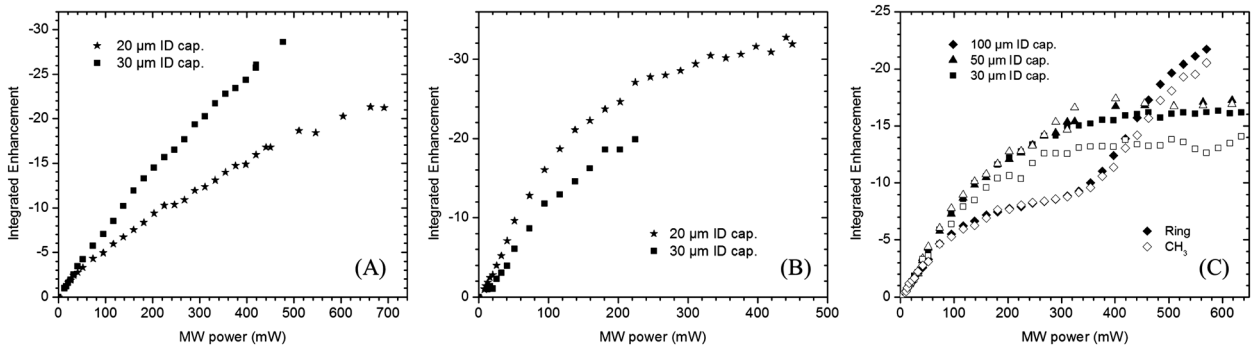

Fig. 3 The DNP enhancement plotted against the incident MW power for 1 M ^{14}N-TEMPOL in DMSO (A) and acetone (B), and 200 mM ^{14}N-TEMPOL in toluene (C) samples. Capillary sizes: 100 (◆), 50 (▲), 30 (■) and 20 µm (★).

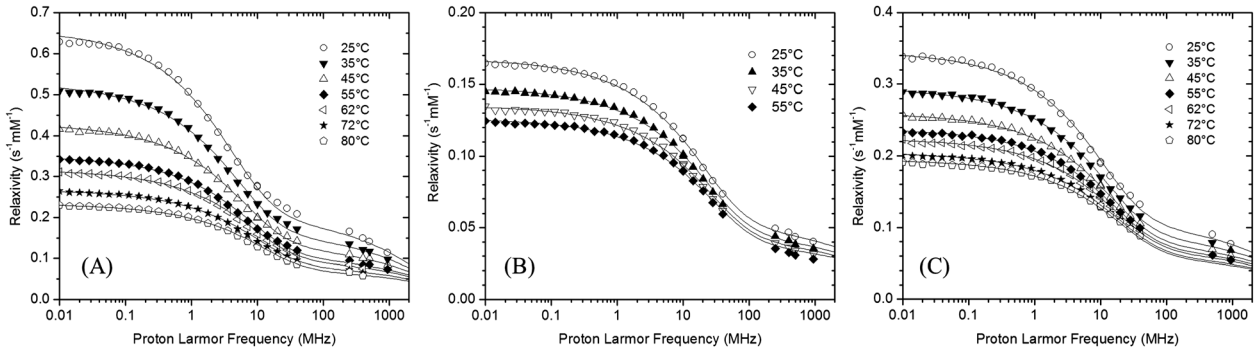

Fig. 4 Solvent ^{1}H relaxivity profiles for solutions of ^{14}N-TEMPOL in DMSO (A), acetone (B) and toluene (C) are shown at different temperatures ranging from 25 to 80 °C. Best fit profiles from the outer-sphere model are also shown as lines.

NMRD measurements performed at temperatures ranging from 25 °C to boiling temperature for all three solvents are shown in Fig. 4.

All dispersion profiles were fitted in a first step by using outer-sphere relaxation only. In this case the free parameter is the translational correlation time τ_D and the relaxivity is given by

$$\frac{R_1}{c} = C(7J(\omega_I, \tau_D) + 3J(\omega_S, \tau_D)) \quad (5)$$

with c being the concentration of radicals, C a constant[8] and R_1 the longitudinal nuclear spin relaxation rate. The fits to the experimental dispersion curves are rather good, although not perfect for DMSO and toluene. The resulting fit parameter τ_D is reported in Table 2 for all solvents and two temperatures (model A). Slightly better fits for DMSO and toluene could be achieved by introducing an additional spectral density from inner-sphere contributions of the transiently formed radical–solvent complex (model B, data and fits shown in the ESI†). The rather small differences in the NMRD fits for these two solvents mainly show up in the region between 20 and 200 MHz proton Larmor frequencies. Note that the data points above 100 MHz are taken in a non-classical way by relaxation measurements on NMR spectrometers at the respective proton Larmor frequencies, leading to larger variations and errors of these data points. For the inner-sphere contributions a Lorentzian spectral density with a correlation time τ_c was considered, with a temperature dependence given by

$$\tau_c = A \cdot \exp(B/T) \quad (6)$$

The values for outer-sphere diffusion correlation time τ_D and inner-sphere correlation time τ_c are reported under model B in Table 2. All best fit parameters are reported in the ESI.† Notably, the diffusion coefficients obtained from the best fit of the NMRD profiles (see Tables S1–S3, ESI†) are in agreement with the values expected for the different solvents. For comparison also the values for water as solvent are given in Table 2. For water satisfactory fits of the NMRD dispersion curves could only be obtained by taking also inner-sphere dynamics into account.[6] For all solvents a strong decrease of both correlation times τ_D and τ_C (about a factor of 2–3) could be observed by an increase of the temperature by 55 °C. For acetone, because of the low boiling temperature, only a temperature increase of 30 °C could be achieved, resulting in a much lower factor of 1.35 only. Thus, increasing the temperature by heating strongly affects the coupling factor ξ and therefore the achievable DNP enhancement ε, as a result of the decrease in the correlation times.

Table 2 Fit parameters of the NMRD profiles. Model A represents fits with only outer-sphere diffusional motion with correlation time τ_D, model B with additional inner-sphere complex motion with an additional correlation time τ_C. In model B, the increase in the paramagnetic enhancement is proportional to $\sum_i n_i/r_i$,[6] where n_i is the number of protons at distance r_i from the paramagnetic center. Due to the six-power dependence, protons at the shortest distance are those providing the largest contribution. Further data are given in the ESI

Solvent molecule	Model	Temperature [K]	Trans. corr. time τ_D [ps]	Inner sphere corr. time τ_C [ps]
DMSO	A	298	115	—
DMSO	A	353	41	—
DMSO	B	298	129	1.57
DMSO	B	353	46	0.55
DMSO	C	298	127	3.71
DMSO	C	353	46	0.29
Acetone	A	298	23	—
Acetone	A	328	17	—
Toluene	A	289	43	—
Toluene	A	353	24	—
Toluene	B	298	49	1.54
Toluene	B	353	28	0.92
Water	B	298	30	17
Water	B	353	11	4

The comparison of the coupling factors predicted from the fits of the NMR dispersion curves and from the DNP enhancements (by taking the saturation factor s and the leakage factor f explicitly into account) is shown for DMSO, acetone and toluene in Fig. 5.

Interestingly, while for the low viscosity solvent acetone the coupling factors extracted from DNP and NMRD measurements agree very well without taking into account any effect from fast τ_c inner-sphere contributions, for the higher viscosity solvents DMSO and toluene inner-sphere fast dynamics of the complex must be explicitly taken into account. However, in the case of DMSO, the NMRD predicted coupling factors are clearly somewhat larger than the DNP determined coupling factors. We have then fit

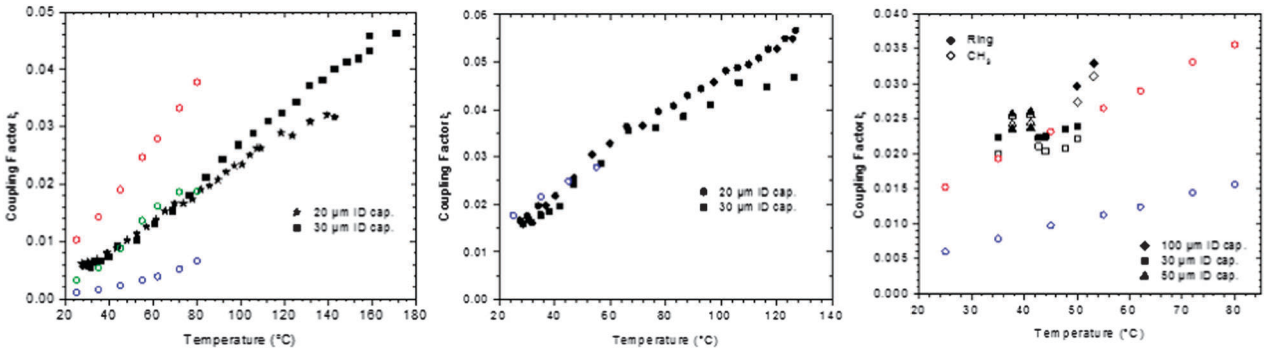

Fig. 5 Comparison of coupling factors ξ calculated from DNP enhancement (in black) and from NMRD (outer-sphere model A in blue, outer-sphere and inner-sphere model B in red, model C as explained in the text in green) as a function of temperature. Left panel: DMSO, middle panel: acetone, right panel: toluene.

the NMRD profiles without imposing eqn (6) and found that an almost equally good fit can be obtained (see model C in Tables S5–S7 and Fig. S13 and S14, ESI†) providing NMRD-derived coupling factors in nice agreement with the DNP data (Fig. 5A). In summary, for DMSO and toluene the fast dynamics of the solvent–radical complex compensate the much lower efficiency of the diffusional dynamics, and contribute significantly to the overall coupling factor and therefore DNP enhancement observed for these solvents. Despite the fact that this high frequency dynamics only contribute rather weakly to the NMR dispersion curves they are essential to explain the high enhancements observed for these two solvents and to get consistent interpretation of DNP and NMRD experiments.

It is interesting to compare the coupling factors ξ calculated from experimental magnetic resonance experiments with the ones extracted from MD simulations.[15,16] For toluene solutions at room temperature MD simulations predict a coupling factor of 0.019 to 0.02 at a magnetic field of 9.2 T for methyl and ring protons, respectively. These values agree very well with the coupling factors calculated from DNP enhancements and from the values predicted from NMRD measurements assuming outer-sphere and inner-sphere relaxation. The small difference of 10% between ring and methyl protons is beyond the accuracy of the DNP measurements, but indeed a slightly larger enhancement could be observed for the ring proton peaks (Fig. 2). Higher DNP enhancement of the ring protons has also been experimentally observed at lower magnetic fields of 0.3 T[17] and 3.4 T.[18] At low radical concentrations (<5 mM) and low magnetic field (0.3 T) higher enhancements were found in toluene compared to water as solvent. The reason is favourable saturation and leakage factors for toluene under these experimental conditions, whereas the extracted coupling factor at such magnetic fields was found to be about 30% lower for toluene compared with water, in good agreement with predictions from our NMRD measurements and MD simulations.[16] Interestingly the situation is opposite at a high magnetic field of 9.2 T: here the leakage and saturation factors at 5 mM radical concentration are slightly less favorable in toluene, whereas the coupling factor is higher for toluene compared to water. This demonstrates that different dynamics contribute to the DNP enhancement at different magnetic field strengths. At low magnetic fields translational diffusion (see Scheme 1 for rates) plays the dominant role, leading to a larger coupling factor for water compared to toluene. At high magnetic fields the very fast inner-sphere dynamics of the nitroxide–toluene complex (compared to the nitroxide–water solution) contributes significantly to the coupling factor (Table 2 and ESI†). The rotational correlation times for nitroxide radicals in toluene extracted from cw-EPR spectra recorded at 9 and 260 GHz are longer than the inner-sphere correlation times necessary to explain our coupling factors at 260 GHz (see ESI†). DNP measurements performed at 94 GHz (3.4 T magnetic field)[18] achieved a maximal enhancement of −45, again in rather good agreement with the respective coupling factors extracted from NMRD or MD[16] data (assuming $f = 1$ and $s = 1$).

Also for DMSO as solvent very fast inner-sphere dynamics are essential to explain the DNP enhancements at high magnetic fields. In this case inner-sphere correlation times somewhat different from those obtained from the best fit to the NMRD profiles have to be assumed to achieve satisfactory agreement with NMRD and DNP data simultaneously. Nevertheless also these correlation times are much shorter than the rotational correlation times extracted from cw-EPR measurements (see ESI†). Similar discrepancies between rotational correlation times and inner-sphere dynamics have also been observed for TEMPOL in ethanol at 3.4 T magnetic field.[19] It can be speculated that low frequency vibrational or librational dynamics of the transient radical–solvent complex might be the source of these fast dynamics modulating the electron–nuclear spin hyperfine interaction on a short ps to sub-ps time scale, which are especially important for the DNP coupling factor at high magnetic fields and which are not modeled well within the approximations made by the force-free hard-sphere model.[16] Molecular dynamic simulations might allow obtaining a more atomistic understanding of such fast local dynamics.

Experimental

CW-EPR measurements were performed with our home built G-band EPR spectrometer operating at a frequency of 180 GHz and a magnetic field of 6.4 T.[20]

DNP experiments were performed on a setup consisting of a commercial 400 MHz NMR spectrometer (Bruker Advance) equipped with a home built EPR bridge operating at 260 GHz

for electron spin excitation.[21] The samples were filled in quartz capillaries (Polymicro) with 100, 50, 30 or 20 μm inner diameter (ID) and an outer diameter of 150 μm and sealed with wax at both ends. They were placed inside a home built double resonance DNP probe with a cylindrical TE_{011} microwave resonator which also acts as a resonant helical coil for the NMR excitation (260 GHz/400 MHz). The length of the MW cavity is approximately 1.6 mm, leading to effective sample volumes of 13, 3, 1.1 or 0.5 nl respectively. Microwave excitation with power of up to 500 mW was achieved by a gyrotron source. The DNP enhancements were determined by taking the ^{1}H FT-NMR spectra of the samples with and without continuous wave (CW) MW irradiation of the central hyperfine line of the ^{14}N-TEMPOL nitroxide spectra. Integrated proton NMR signals were used to calculate the DNP enhancement factor ε. The temperature is a critical parameter in the DNP experiments because of sample heating by the microwave excitation. We determined the sample temperature of the tiny DNP samples under microwave irradiation by the temperature dependent chemical shift difference ($\Delta\delta$) between the CH_2 and OH groups of ethylene glycol.[6] We added 10% of ethylene glycol to pure solvent samples and recorded the shift difference ($\Delta\delta$) as a function of temperature using the Bruker BBI probe. Subsequently, $\Delta\delta$ was monitored in the DNP resonator under microwave irradiation, allowing determination of the sample temperature at a given microwave power. We observed a very strong MW heating in the case of acetone (similar to water) and smaller microwave heating with the other two solvents. We estimated the error in the temperature determination by this method to be less than 10%. While we could use ethylene glycol as a "chemical shift thermometer" in the case of DMSO, acetone and water, this method failed in the case of toluene, because of insolubility. Unfortunately, also methanol as a substitute for ethylene glycol could not be used successfully because NMR signals outside the MW resonator overlapped with the methanol lines. However toluene, among all the above mentioned solvents, has the lowest dielectric constant and therefore very low MW heating. Together with the knowledge gained on the other solvents we could estimate the temperature of toluene to be below 60 °C even under high microwave excitation power. This was also confirmed by DNP experiments performed with different ID capillaries (as shown in Fig. 2C). For the two smaller capillaries (30 and 50 μm) we observed the same rise of the enhancement upon applied MW power, demonstrating that we observe a rise due to the change in the saturation factor and not due to elevated temperature for such capillary sizes. In the largest capillary (100 μm) we saw a step in the enhancement curve which is also observable in the paramagnetic NMR shift measurements (see ESI†). This might be due to detuning of the microwave resonant cavity by heating or convection flow in the larger capillary. Due to the larger dielectric losses in DMSO and acetone, we performed all the DNP experiments in 20 μm and 30 μm ID capillaries (Fig. 2A and B). DMSO shows the expected trend, where the enhancement in the larger capillary rises faster than in the smaller one, due to heating. However this is not the case with acetone, where we see an opposite effect due to different saturation behaviour (see ESI†).

Relaxation time measurements were performed using a commercial 400 MHz liquid state probe (Bruker BBI). Longitudinal relaxation rates at magnetic fields ranging from 0.01 to 40 MHz proton Larmor frequency were measured using the field cycling technique with a high sensitive relaxometer (Stelar Spinmaster FFC-2000-1T). Errors in the measurement of the relaxation rates were below 1%. Proton relaxivity was calculated by subtraction of the relaxation rates of the buffer from the relaxation rate of the ^{14}N-TEMPOL solution, and normalization to the radical concentration. High frequency relaxation rates at higher frequencies (250, 400, 500 and 950 MHz) were measured on separate NMR spectrometers.

Conclusion

DNP and NMRD experiments on solutions of TEMPOL radicals in DMSO, acetone and toluene have been performed. The coupling factors ξ extracted from these measurements range between 0.005 and 0.02 at room temperature, despite their order of magnitude different viscosities and diffusion constants. Thus, large proton Overhauser DNP enhancements in the range of 10–50 have been observed for all three solvents. This is in line with experimental results on the polarization transfer efficiency from TEMPOL to water[6] or other molecules such as pyruvate, lactate and acetate in aqueous solution.[22] In all these cases substantial DNP enhancements could be observed at a high magnetic field of 9.2 T. A combination of the two methods allows one to highlight and quantify the significant contribution of fast dynamics of the radical–solvent complex to the coupling factor at high magnetic fields not related to viscosity and translational diffusion coefficient of the solvent and the radical molecule. Molecular dynamic simulations might give more insight into the molecular origins of these fast dynamics and allow one to make predictions for optimization of the DNP agent/target system for a given magnetic field strength. These findings also allow one to speculate that liquid state Overhauser DNP polarization transfer might be efficient and useable at even higher magnetic field strengths, provided the technical problems related to MW sample heating can be solved.

Acknowledgements

This work was supported by the DIP program from the German Research Council (DFG), the Center for Biomolecular Magnetic Resonance (BMRZ), Frankfurt, the European Commission (Bio-NMR) and the COST Action (TD1103). We would like to thank Juan Carlos Lagomacini for checking the temperature calibration procedure, Burkhard Endeward, Johanna Baldus, Christian Richter, and Frank Löhr for experimental assistance and Shimon Vega for scientific discussion. Also, we gratefully acknowledge technical support from Bernhard Thiem, Manfred Strupf and Bruker Biospin.

References

1 L. R. Becerra, G. J. Gerfen, R. J. Temkin, D. J. Singel and R. G. Griffin, *Phys. Rev. Lett.*, 1993, **71**, 3561–3564.
2 J. H. Ardenkjær-Larsen, B. Fridlund, A. Gram, G. Hansson, L. Hansson, M. H. Lerche, R. Servin, M. Thaning and

K. Golman, *Proc. Natl. Acad. Sci. U. S. A.*, 2003, **100**, 10158–10163.
3 M. J. Prandolini, V. P. Denysenkov, M. Gafurov, B. Endeward and T. F. Prisner, *J. Am. Chem. Soc.*, 2009, **131**, 6090–6092.
4 C. Griesinger, M. Bennati, H. M. Vieth, C. Luchinat, G. Parigi, P. Höfer, F. Engelke, S. J. Glaser, V. Denysenkov and T. F. Prisner, *Prog. Nucl. Magn. Reson. Spectrosc.*, 2012, **64**, 4–28.
5 A. W. Overhauser, *Phys. Rev.*, 1953, **92**, 411–415.
6 P. Neugebauer, J. G. Krummenacker, V. P. Denysenkov, G. Parigi, C. Luchinat and T. F. Prisner, *Phys. Chem. Chem. Phys.*, 2013, **15**, 6049–6056.
7 L.-P. Hwang and J. H. Freed, *J. Chem. Phys.*, 1975, **63**, 4017–4025.
8 M.-T. Turke, G. Parigi, C. Luchinat and M. Bennati, *Phys. Chem. Chem. Phys.*, 2012, **14**, 502–510.
9 I. Bertini, C. Luchinat and G. Parigi, *Adv. Inorg. Chem.*, 2005, **57**, 105–172.
10 D. Sezer, M. J. Prandolini and T. F. Prisner, *Phys. Chem. Chem. Phys.*, 2009, **11**, 6626–6637.
11 W. R. Baird and R. T. Foley, *J. Chem. Eng. Data*, 1972, **17**, 355–357.
12 S. Glasstone, *Textbook of Physical Chemistry*, Macmillan & Co Ltd, London, 1951.
13 R. Battino, T. R. Rettich and T. Tominaga, *J. Phys. Chem. Ref. Data*, 1983, **12**, 163–178.
14 I. Bertini, C. Luchinat and G. Parigi, *Solution NMR of Paramagnetic Molecules*, Elsevier, 2001, vol. 2.
15 D. Sezer, *Phys. Chem. Chem. Phys.*, 2013, **15**, 526–540.
16 D. Sezer, *Phys. Chem. Chem. Phys.*, 2014, **16**, 1022–1032.
17 N. Enkin, G. Liu, I. Tkach and M. Bennati, *Phys. Chem. Chem. Phys.*, 2014, **16**, 8795–8800.
18 E. V. Kyukov, M. E. Newton, K. J. Pike, D. R. Bolton, R. M. Kowalczyk, A. P. Howes, M. E. Smith and R. Dupree, *Phys. Chem. Chem. Phys.*, 2010, **12**, 5757–5767.
19 G. H. A. van der Heijden, A. P. M. Kentgens and P. J. M. van Bentum, *Phys. Chem. Chem. Phys.*, 2014, **16**, 8493–8502.
20 M. H. Hertel, V. Denysenkov, M. Bennati and T. F. Prisner, *Magn. Reson. Chem.*, 2005, **43**, 248–255.
21 V. P. Denysenkov, M. J. Prandolini, M. Gafurov, D. Sezer, B. Endeward and T. F. Prisner, *Phys. Chem. Chem. Phys.*, 2010, **12**, 5786–5790.
22 J. Krummenacker, V. Denysenkov and T. F. Prisner, *Appl. Magn. Reson.*, 2012, **43**, 139–146.